AIP Journal of Renewable and Sustainable Energy

Free . Submitted: 22 March 2021 . Accepted: 21 June 2021 . Published Online: 21 July 2021

Wind farm yaw control set-point optimization under model parar uncertainty

Journal of Renewable and Sustainable Energy **13**, 043303 (2021); https://doi.org/10.1063/5.0051071

Michael F. Howland[a)]

View Affiliations

TOPICS

- Turbulence simulations
- Optimization algorithms
- Wind energy
- Probability theory
- Mathematical modeling
- Measuring instruments
- Atmospheric dynamics
- Wind turbines
- Energy harvester

ABSTRACT

Wake steering, the intentional yaw misalignment of certain turbines in an array, has demonstrated potential as a wind farm control approach to increase collective power. Existing algorithms optimize the yaw misalignment angle set-points using steady-state wake models and either deterministic frameworks or optimizers that account for wind direction and yaw misalignment variability and uncertainty. Wake models rely on parameterizations of physical phenomena in the mean flow field, such as the wake spreading rate. The wake model parameters are uncertain and vary in time at a wind farm depending on the atmospheric conditions, including turbulence intensity, stability, shear, veer, and other atmospheric features. In this study, we develop a yaw set-point optimization approach that includes model parameter uncertainty in addition to wind condition variability and uncertainty. To enable computationally efficient online set-point optimization under model parameter uncertainty, a simplified, approximate parameter distribution estimation method is used. The optimization is tested in open-loop control numerical experiments using utility-scale wind farm operational data for which the set-point optimization framework with parametric uncertainty has a statistically significant impact on the wind farm power production for certain wind turbine layouts at low turbulence intensity, but the results are not significant for all layouts considered nor at higher turbulence intensity. The set-point optimizer is also tested for closed-loop wake steering control of a model wind farm in large

eddy simulations of a convective atmospheric boundary layer (ABL). The yaw set-point optimization with model parameter uncertainty reduced the sensitivity of the closed-loop wake steering control to increases in the yaw controller update frequency. Increases in wind farm power production were not statistically significant due to the high ambient power variability in the turbulent, convective ABL.

I. INTRODUCTION

The intentional yaw misalignment of leading wind turbines to deflect the energy deficit wake region away from downwind generators,[1] termed wake steering, has emerged as a promising collective control strategy to increase wind farm power production.[2] The initial approach to wake steering in field experimental studies leverages open-loop control, where optimal yaw misalignment set-points are computed offline for each turbine as a function of averaged wind conditions and are provided to the wind turbines in a discrete lookup table format.[3] While open-loop wake steering control has demonstrated potential in large eddy simulations (LES)[2] and field experiments[3–6] to increase wind farm power production, control methodologies which are designed for variations in the atmospheric boundary layer (ABL) wind conditions require further development to reliably increase annual energy production (AEP).[7]

Wind conditions, including wind speed, wind direction, turbulence intensity (TI), and atmospheric stability, change as a function of time in the ABL. During the diurnal evolution of the ABL, modifications to the surface heat flux by solar heating alter the boundary layer structure and wind conditions.[8] Further, with fixed boundary conditions, the turbulent nature of the ABL results in chaotic flows which depend on the initial conditions, requiring ensemble averages to converge statistical quantities based on the instantaneous states, including turbine power production. As a result, even within narrow wind condition bins in an open-loop lookup table, a variety of instantaneous wind farm power outcomes will occur. Beyond variability within a wind condition bin, high-frequency variations in the wind speed and direction occur above the low-pass filter cutoff frequency of averaged conditions and optimal yaw misalignment set-point calculations should consider these variability contributions rather than utilizing deterministic mean wind conditions.[9,10] Aside from natural condition variability, wind turbine sensors which measure flow conditions, such as nacelle-mounted wind vanes or anemometers, are inherently noisy and imperfect,[11,12] introducing further wind condition uncertainty in active wake control.

Yaw misalignment set-point optimization is typically performed with steady-state wake models which represent time-averaged flow behavior.[2] Model-based yaw set-point optimization has been performed using game-theoretic approaches based on random yaw perturbations,[2,13] finite-difference gradient-based sequential least squares programming,[14] COBYLA optimization,[15,16] and analytic gradient-based optimization.[5,17] The steady-state wake models estimate $\boldsymbol{P}_{\infty}$, the infinite time average of the power production of the wind farm with fixed wind conditions, including wind speed and wind direction, and fixed turbine

control decisions, including yaw misalignment. This modeling approach assumes an inherent scale separation between turbine-induced flow adjustment and atmospheric condition changes. Initial wake steering experiments used steady-state wake models to optimize the yaw set-points with deterministic, fixed wind conditions.[2] In a wake steering application, the wind conditions may have high-frequency, turbulent variations and low-frequency atmospheric condition variations. Such variations are not directly modeled using a steady-state wake model with deterministic wind conditions, which may introduce model bias when applying a steady-state wake model to low-pass filtered (e.g., 10 min averaged) wind conditions.

Recent studies have extended model-based yaw set-point optimization to maximize the expected value of the power production given wind condition or turbine control system variations and uncertainty. Quick *et al.*[9] used a steady-state wake model and formulated the wake steering yaw set-point calculation as optimization under uncertainty with yaw deviations from the set-point value. Rott *et al.*[18] formulated the set-point calculation as optimization under wind direction uncertainty (termed robust optimization), rather than with fixed, deterministic incident winds. The high-frequency wind direction variations above the yaw controller low-pass filter cutoff (5 min in Rott *et al.*[18]) were modeled by a Gaussian probability density function based on field measurements. Simley *et al.*[19] extended the robust set-point optimization to include natural yaw misalignment variability due to slowly evolving yaw control systems. Finally, Quick *et al.*[16] used polynomial chaos expansion to solve the yaw set-point optimization under uncertainty problem with the addition of stochastic turbulence intensity and shear and found that the uncertain wind direction had the largest impact on the set-point optimization results.

Steady-state wake models introduce a number of assumptions and parameterizations in order to analytically represent time-averaged wake behavior. The power production prediction from the resulting wake models relies on the empirical calibration of the parameters, which represent key features of the flow, including the wake spreading rate.[20] However, empirical calibrations using idealized LES or wind tunnel experiments introduce error and uncertainty in field deployments, where the flow physics exhibits different forcings, such as Coriolis forces, stratification, and terrain complexity. Here, we introduce a difference between wind conditions, such as wind direction and speed, and wake model parameters, such as the wake spreading rate, which parameterizes physical phenomena. The wake model parameters depend on the inflow conditions, but the exact functional dependence is not known. Wake model parameters have been tuned using LiDAR field data[21] and neutral ABL LES flow fields.[22] Recent work has optimized the wake model parameters using only wind farm power data and analytic gradients,[5] least squares fitting,[23] genetic algorithms,[24] and Kalman filtering[17] and demonstrated that assimilating operational wind farm data into the wake model improves its predictive capability. Zhang and Zhao[25] used sampling to approximate the Bayesian posterior distributions of wake model parameters given LES data as the ground truth. Using the wake model parameter posteriors, a stochastic

wake model based on uncertain model parameters was proposed which improved predictions compared to wake modeling with deterministic model parameters. Wake model error correction terms have also been proposed[26] and learned using operational data, which improved wake model predictions.

Recent studies have developed closed-loop methodologies to improve model-based wake steering control in temporally evolving wind conditions. The yaw misalignment values applied to the wind farm are updated in time with wind conditions[27] and wake model parameters[17] estimated through the assimilation of finite time-averaged wind farm data. Kanev[28] demonstrated that the energy gain from closed-loop wake steering control is sensitive to the control update frequency.

The incorporation of model parameter uncertainty in yaw misalignment set-point optimization is anticipated to reduce the sensitivity of the yaw set-points to noisy, finite time-averaged wind farm data. While model parameter uncertainty is relevant for both open- and closed-loops model-based control, yaw set-point optimization which considers model parameter uncertainty is anticipated to be more critical when applying closed-loop control due to limited statistical averaging and additional wind condition uncertainty.[17] In this paper, we extend yaw misalignment set-point optimization methods to include model parameter uncertainty, where the wake model is optimized based on a probability distribution of wake model parameters rather than deterministic values. We first develop a yaw set-point optimization based on stochastic programming[29] including wake model parameter and wind condition uncertainty. The yaw set-point optimization can be used with arbitrary parameter distribution estimate methods. We use a simple methodology to estimate an approximate probability distribution of the uncertain wake model parameters without using computationally expensive Bayesian posterior sampling methods, such as Markov chain Monte Carlo (MCMC).[30] The simple estimate assumes that the probability distribution of the parameters can be approximated by the probability distribution of the power production data, which is inexact due to the nonlinear model mapping and due to model error, which is neglected in the simple approach. The estimated model parameter distributions are used in tandem with the wind condition distributions in the stochastic programming approach.

To test the performance of the stochastic approach, two distinct numerical experiments are performed. Using supervisory control and data acquisition (SCADA) data from a utility-scale wind farm, numerical wake model experiments are performed to represent open-loop wake steering. The wind farm operational data are used offline to construct yaw set-point lookup tables as a function of the wind conditions for deterministic and optimization under uncertainty. The approaches are tested using the wake model as a surrogate wind farm, where the model is locally fit to time series SCADA data, to test open-loop control performance. This experiment can be viewed as an idealized, perfect model setting, where the same wake model is used for yaw set-point lookup table construction and for simulations. Therefore, there is no inherent model error, only variations in wind conditions

and model parameters in the time series. Additionally, the set-point optimization method is tested using closed-loop wake steering control in LES of an unstable, convective ABL. The LES has inherent wind condition variations due to the turbulent, convective ABL. These experiments include potential model discrepancy when applying the steady-state wake model to predict LES power production, compared to the perfect model setting open-loop experiments.

The yaw misalignment set-point optimization formulation under wind condition variability and model parameter uncertainty is given in Sec. II. The wake model is discussed in Sec. II A and the simple parameter probability distribution estimation methodology is introduced in Sec. II B. In Sec. III, wake steering numerical case studies of a utility-scale wind farm using operational data are performed. LES simulations of closed-loop control of a model wind farm in convective ABL conditions are performed in Sec. IV. Conclusions are given in Sec. V.

II. YAW SET-POINT OPTIMIZATION UNDER MODEL PARAMETER UNCERTAINTY

The goal of wake steering is to maximize wind farm power production through the use of intentional yaw misalignment. For open-loop control, the goal is to calculate the optimal yaw misalignment set-points for each wind condition bin, specified by wind speed, turbulence intensity, and wind direction.[4] For wake model-based closed-loop control (e.g., the method proposed by Howland *et al.*[17]), the goal is to calculate the optimal yaw set-points for the wind farm over the finite control update time horizon. In both approaches, the set-point optimization can be considered over wind condition probabilities. The wind condition probabilities are pretabulated in the open-loop setting. In closed-loop control, the wind condition probabilities are collected online, as wind condition and power measurements over the previous finite time control update horizon.

Given variability and uncertainty in the wind conditions $\boldsymbol{c}$ and wake model parameters $\boldsymbol{\psi}$, this optimization goal is to select the yaw misalignment set-points $\boldsymbol{\gamma}_s$ which maximize the expected value of the power production,

$$\boldsymbol{\gamma}_s^*(\boldsymbol{c}, \boldsymbol{\psi}) = \text{argmax}_{\boldsymbol{\gamma}_s} \mathbb{E}\left[\mathcal{G}(\boldsymbol{c}, \boldsymbol{\psi}, \boldsymbol{\gamma}_s)\right], \tag{1}$$

where $\mathcal{G}(\boldsymbol{c}, \boldsymbol{\psi}, \boldsymbol{\gamma}_s)$ is the wind farm power production. The optimal yaw misalignment set-points over the wind turbines in the farm is $\boldsymbol{\gamma}_s^*$. The expected value of the power production is given by an integration over the wind condition and wake model parameter spaces,

$$\mathbb{E}\left[\mathcal{G}(\boldsymbol{c}, \boldsymbol{\psi}, \boldsymbol{\gamma}_s)\right] = \int \cdots \int f(\boldsymbol{c}) f(\boldsymbol{\psi}) \mathcal{G}(\boldsymbol{c}, \boldsymbol{\psi}, \boldsymbol{\gamma}_s) d\boldsymbol{c}\ d\boldsymbol{\psi}, \tag{2}$$

where $f(\boldsymbol{\psi})$ is the probability density function over the wake model parameter space $\boldsymbol{\psi}$ and $f(\boldsymbol{c})$ is the probability density function over the wind condition space $\boldsymbol{c}$. The computationally efficient analytic gradient-based optimizer developed by Howland *et al.*[5] is extended to the stochastic programming problem in Eq. (1) and is used in this study. Analytic gradients of the wind farm power production with respect to the yaw misalignment set-points $(\partial \mathcal{G}/\partial \gamma_s)$ are

wind farm power production with respect to the yaw misalignment set-points ($\partial J/\partial \boldsymbol{\gamma}_s$) are computed from the wake model using a successive application of the chain rule (see analytic gradient derivation in Howland *et al.*[5] and Howland and Dabiri[31]). The wind condition and parametric uncertainty are incorporated by weighting the gradients with the probability associated with the values of wind conditions and model parameters in use in the wake model realization. The probability weighting results from the integration technique in use, e.g., simple quadrature,[19] Monte Carlo integration, or polynomial chaos expansion.[16] In this study, we use a simple quadrature approach.[19] While the use of a gradient-based optimization routine for a non-convex problem [Eq. (1)] does not guarantee a globally optimal solution,[32,33] the optimization in practice finds satisfactory local optima at a low computational cost[5] compared to gradient-free methods. For open-loop control, Eq. (2) will be solved for each wind condition bin; while for closed-loop control, Eq. (2) will be solved at each control update step in an online fashion.[17]

The probability distributions of the wake model parameters can be estimated using approximate Bayesian inference methods, such as Markov chain Monte Carlo.[25,30] However, sampling-based methods are computationally intensive, often requiring $\mathcal{O}(10^5)$ forward model evaluations to perform the Bayesian inverse problem analysis for complex models.[30] This requirement becomes challenging for on-the-fly estimation of wake model probability densities in closed-loop control. Instead, in this study (Sec. II B), we will develop a simple method to estimate an approximate wake model parameter probability distribution to be used in Eq. (2) based on power production data by leveraging parameter estimation techniques.

Previous approaches estimated the wake model parameters based on an average of the power within a wind condition bin.[5] The SCADA operational data also has underlying uncertainty and variability, for example, from physical effects such as dynamic wake meandering and statistical effects from finite time averaging, which corresponds to uncertainty and variability in the wake model parameters represented by the probability function $f(\boldsymbol{\psi})$. The probability density functions will be defined specifically for each wind condition bin based on the utility-scale wind farm data in Sec. III A and for LES data in Sec. IV.

The optimization framework is shown in Fig. 1. In practice, Eq. (2) is discretized to solve using the analytic wake model.[9,18] While other expectation calculation methods could be used, such as polynomial chaos expansion,[16] direct quadrature is used in this study for simplicity and due to the computational efficiency of the gradient-based set-point optimization.[5] The discretization, along with the prescribed wind condition uncertainty,[18] becomes additional hyperparameters. In Sec. III C, we will analyze the sensitivity of wake steering to these hyperparameters.

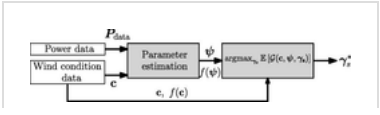

FIG. 1. Set-point optimization under model parameter uncertainty. The wake model parameters $\boldsymbol{\psi}$ are

estimated by the ensemble Kalman filter (EnKF) for a set of wind conditions $\boldsymbol{c}$ and averaged power data $\boldsymbol{P}_{\text{data}}$. The probability distribution of the parameters $f(\boldsymbol{\psi})$ is derived from the power data and used in tandem with the condition probability distributions $f(\boldsymbol{c})$ to compute $\boldsymbol{\gamma}_s^*$ with set-point optimization [Eq. (1)].

A. Steady-state wake model

The nonlinear wake model used in the present study, denoted by $\mathcal{G}$, is the lifting line model;[34] however, the methods described below can be used for arbitrary steady-state wake models. The wake model represents the time-averaged wake region trailing yaw misaligned or yaw-aligned turbine and was validated against experimental data.[34] The model has been used in subsequent wake steering power optimization studies in LES[17] and field experiments.[5] The wake model predicts wind farm power for arbitrary inflow wind conditions and wind turbine layout given two physics-based parameters, $\boldsymbol{k_w}$ and $\boldsymbol{\sigma_0}$, which denote the wake spreading rate and the proportionality constant for the presumed Gaussian wake profile. The area-averaged velocity deficit at a downwind turbine j as a result of the wake of an upwind turbine i is

$$\Delta u_{i,j}(x) = \frac{\sqrt{2\pi}\delta u_i(x) d_{w,i}(x) D}{16\sigma_{0,i}} \left[\operatorname{erf}\left(\frac{y_T + D/2 - y_{c,i}(x)}{\sqrt{2}\sigma_{0,i} d_{w,i}(x)} \right) - \operatorname{erf}\left(\frac{y_T - D/2 - y_{c,i}(x)}{\sqrt{2}\sigma_{0,i} d_{w,i}(x)} \right) \right], \tag{3}$$

where D is the turbine diameter, x is the streamwise direction, y_T is the lateral turbine centroid of turbine j, and the streamwise velocity deficit[31,34] is

$$\delta u_i(x) = \frac{2 a_i u_{0,i}}{d_{w,i}^2(x)} \frac{1}{2} \left[1 + \operatorname{erf}\left(\frac{x}{\sqrt{2} D/2} \right) \right], \tag{4}$$

with $u_{0,i}$ as the effective (rotor area averaged) velocity perceived by turbine i and axial induction factor a_i. The wake diameter is $d_w(x) = 1 + k_w \log\left(1 + \exp\left[2(x/D - 1)\right]\right)$. The wake centroid $y_{c,i}$ is a function of the yaw misalignment of the upwind turbine i. Details on the wake deflection model are given in Shapiro *et al.*[34] In the open-loop numerical experiments, linear superposition is used.[35] In the LES case studies, the improved modified linear wake superposition[20] is used since its performance is similar to the more computationally expensive momentum conserving superposition.[31,36] The rotor area-averaged velocity at turbine j is

$$u_{e,j} = u_\infty - \sum_i^{N_f} \Delta u_{i,j}, \tag{5}$$

where N_f is the number of upwind turbines and the power production is $\widehat{P}_j = \frac{1}{2}\rho A C_{P,j} u_{e,j}^3$ with $C_{P,j}$ estimated from a power curve. The incident velocity to the wind farm is u_∞. In this

study, $C_{P,j} = C_{P,j}(\gamma_s = 0) \cdot \cos^{P_p}(\gamma_{s,j})$ is used although the recently developed blade-element model which accounts for wind velocity profiles could be used in future studies with rotational turbine models.[37] For the utility-scale wind farm numerical experiments, $P_p = 2$, which represents a reasonable first order approximation of $C_{p,j}(\gamma_{s,j})$ as shown in a yaw misalignment field experiment at the same wind farm.[37] For the LES experiments, P_p was set to 2.5 based on empirical tuning. The secondary steering model proposed by Howland and Dabiri[31] is used. Aside from the wake model parameters, the predicted power production of a wind farm depends on the turbine layout,[38] the incident wind speed u_∞, the wind direction, and the turbine yaw misalignment set-points $\boldsymbol{\gamma}_s$. Additionally, there may be deviation from the yaw set-point for each turbine due to yaw error[9] which is denoted as $\boldsymbol{\zeta}$. The yaw error $\boldsymbol{\zeta}$ represents a deviation from the intended yaw set-point ($\boldsymbol{\gamma}_s$) as a result of local spatiotemporal turbulence. The wind and turbine control conditions are collected into the vector $\boldsymbol{c} = [u_\infty, \alpha, \boldsymbol{\zeta}]$, with wind direction given by α. The effects of turbulence intensity (TI) are included implicitly in the wake model parameters $\boldsymbol{\psi}$ (see Sec. II B). Therefore, TI is not included explicitly in $\boldsymbol{c}$.

The wake model power predictions are collected into a vector and are denoted compactly as $\mathscr{P}(\boldsymbol{c}, \boldsymbol{\psi}, \boldsymbol{\gamma}_s) = [\widehat{P}_1, \ldots, \widehat{P}_{N_t}] \in \mathrm{IR}^{N_t}$, where N_t is the number of turbines in the farm, $\widehat{P}_i$ is the wake model power estimate for turbine i, and

$$\mathscr{G}(\boldsymbol{c}, \boldsymbol{\psi}, \boldsymbol{\gamma}_s) = \sum_{i=1}^{N_t} \mathscr{P}_i(\boldsymbol{c}, \boldsymbol{\psi}, \boldsymbol{\gamma}_s). \tag{6}$$

The wake model predictions depend on two types of inputs: the wind conditions $\boldsymbol{c}$ and the wake model parameters $\boldsymbol{\psi}$,

$$\boldsymbol{\psi} = \left[k_{w,1}, \ldots, k_{w,N_t}, \sigma_{0,1}, \ldots, \sigma_{0,N_t}\right]. \tag{7}$$

B. Approximate wake model parameter probability distribution estimation

In this study, the wake model parameters are estimated using the ensemble Kalman filter (EnKF)[39] and SCADA power production data. Previous studies have used the EnKF to estimate the mean wake model parameters[17,40] and the wake model state.[41,42] For parameter estimation, the EnKF can be viewed as an approximation of gradient-based optimization without requiring direct gradient calculations.[43] The power production SCADA data are measured in finite time averages (e.g., 1 min averages), denoted by $\widetilde{\boldsymbol{P}} \in \mathrm{IR}^{N_t}$. Steady-state wake models estimate $\boldsymbol{P}_\infty$, the infinite time average of the power. However, $\boldsymbol{P}_\infty$ is not available in measurements. Instead, the finite time averages $\widetilde{\boldsymbol{P}}$, which are subject to noise, are used. Following the central limit theorem, the relationship between the infinite time average $\boldsymbol{P}_\infty$ and finite time-averaged realizations $\widetilde{\boldsymbol{P}}$ is

$$\widetilde{\boldsymbol{P}} = \boldsymbol{P}_\infty + N(0, \Sigma_p) \tag{8}$$

$$\widetilde{\boldsymbol{P}} = \boldsymbol{P}_\infty + N(0, \Sigma_P), \tag{6}$$

where N denotes a normal distribution with zero mean and covariance Σ_P. We assume that the variations in the averaged power realizations are the result of the finite time averaging, rather than a localized sensor bias, which may be considered in future work. In practice, the infinite time average of the power production $\boldsymbol{P}_\infty$ has a functional dependence on the incident wind conditions. In field data, this effect is approximated using conditional averaging techniques,[5] where the data are grouped by wind condition bins and then the power data samples are averaged in each bin. Since the steady-state wake model predicts $\boldsymbol{P}_\infty$, we will use the underlying variability in finite time average SCADA power data samples $\widetilde{\boldsymbol{P}}$ to estimate the probability distributions of the wake model parameters.

In order to approximate the wake model parameter probability distribution $f(\boldsymbol{\psi})$, the wake model parameters are estimated using the EnKF for various values of turbine power $\widetilde{\boldsymbol{P}}/\widetilde{P}_1$ within the empirically measured SCADA power probability distribution $[f(\widetilde{\boldsymbol{P}})]$, where $\widetilde{P}_1$ is the finite time average of power for a freestream turbine at the farm. The probability distribution of $\widetilde{\boldsymbol{P}}$ is assumed to be Gaussian with an empirically measured mean and standard deviation. The Gaussian assumption is a reasonable approximation through the central limit theorem, although it will not be exact due to the influence of the varying state of the atmospheric conditions such as thermal stability or heterogeneous flow field effects, which are not accounted for in the standard conditional averaging techniques.[4,5] The Gaussian approximation will be tested using field data in Sec. III A. The power distribution is discretized between $\overline{\boldsymbol{P}} \pm \boldsymbol{\sigma_p}$, where $\overline{\boldsymbol{P}} = \langle \widetilde{\boldsymbol{P}} \rangle$ is the mean of instances within the wind condition bin ($\langle\cdot\rangle$ denoting bin average) and $\boldsymbol{\sigma_p}$ is the corresponding standard deviation. The wake model parameters $\boldsymbol{k_w}$ and $\boldsymbol{\sigma_0}$ are estimated using the EnKF for each power value in the discretized probability distribution. The probability distribution associated with the resulting wake model parameters is assumed to be the same as the empirical power probability distribution and is used in the solution of Eq. (1) using numerical integration. This is an inexact approximation due to the nonlinear model and due to model error, which is neglected in this study. Future work should investigate improved wake model parameter distribution methods which are computationally tractable for closed-loop wake steering control.

Each turbine in the farm has distinct values for the model parameters, since the values depend on the turbine inflow conditions and turbine layout.[44] For N_t wind turbines, the model parameters are $\boldsymbol{\psi} = [k_{w,1}, \ldots, k_{w,N_t}, \sigma_{0,1}, \ldots, \sigma_{0,N_t}]$ [Eq. (7)]. The model parameters are initialized using their standard values reported in the literature[34] of $k_w = 0.1$ and $\sigma_0 = 0.25$. The wind farm layout is rotated according to the incident wind direction. The wake model parameters for downwind turbines whose wakes do not impact other generators are neglected in the estimation. The errors associated with the modeling and measurement are given by $\chi = [\chi_{k_w}^T, \chi_{\sigma_0}^T]^T \in \mathrm{IR}^{2N_t}$ and $\varepsilon \in \mathrm{IR}^{N_t}$, respectively. The errors have prescribed variances and zero mean. The modeling errors have variances of $\sigma_{k_w}^2 = 0.0009$ and $\sigma_{\sigma_0}^2 = 0.0009$. The parameter variances for the Gaussian prior distribution are

hyperparameters and were selected based on tuning experiments.[17] Perturbations are added to the SCADA power production data for each ensemble[45] $\boldsymbol{\xi}^{(i)} = \widetilde{\boldsymbol{P}}_s + \boldsymbol{\varepsilon}^{(i)}$, where $^{(i)}$ denotes ensemble i and $\widetilde{\boldsymbol{P}}_s$ is a sample from the empirical distribution of power data $\widetilde{\boldsymbol{P}}$ and $\boldsymbol{\varepsilon}^{(i)}$ are independent realizations of the noise $N(0, \Sigma_P)$. The perturbed power production ensemble and noise matrix are given by

$$\Xi = \left[\boldsymbol{\xi}^{(1)}, \ldots, \boldsymbol{\xi}^{(N_e)}\right], \qquad \Sigma = \left[\boldsymbol{\varepsilon}^{(1)}, \ldots, \boldsymbol{\varepsilon}^{(N_e)}\right], \tag{9}$$

where N_e is the number of ensembles.

The ensemble of wake model parameters is

$$\Psi = \left[\boldsymbol{\psi}^{(1)}, \ldots, \boldsymbol{\psi}^{(N_e)}\right] \in \mathrm{IR}^{2N_t \times N_e}. \tag{10}$$

The wake model ensemble power predictions are collected in the matrix $\widehat{\Pi} \in \mathrm{IR}^{N_t \times N_e}$. The wake model parameter and power production ensemble means are $\overline{\Psi} = \Psi \mathbf{1}_{N_e}$, and $\overline{\widehat{\Pi}} = \widehat{\Pi} \mathbf{1}_{N_e}$, where $\mathbf{1}_{N_e} \in \mathrm{IR}^{N_e \times N_e}$ is a matrix with all entries as $1/N_e$. Perturbation matrices are given by $\Psi' = \Psi - \overline{\Psi}$ and $\widehat{\Pi}' = \widehat{\Pi} - \overline{\widehat{\Pi}}$.

The intermediate forecast step is

$$\Psi_+ = \left[\boldsymbol{\psi}^{(1)} + B\boldsymbol{\chi}^{(1)}, \ldots, \boldsymbol{\psi}^{(N_e)} + B\boldsymbol{\chi}^{(N_e)}\right], \tag{11}$$

$$\widehat{\Pi}_+ = \left[\mathscr{P}(\boldsymbol{\psi}^{(1)} + B\boldsymbol{\chi}^{(1)}), \ldots, \mathscr{P}(\boldsymbol{\psi}^{(N_e)} + B\boldsymbol{\chi}^{(N_e)})\right], \tag{12}$$

with $B \in \mathrm{IR}^{2N_t \times 2N_t}$ prescribed as the identity matrix. The measurement analysis step is

$$\Psi_p = \Psi_+ + \Psi'_+ \widehat{\Pi}'^T_+ \left(\widehat{\Pi}'_+ \widehat{\Pi}'^T_+ + \Sigma\Sigma^T\right)^{-1} \cdot (\Xi - \widehat{\Pi}_+). \tag{13}$$

The EnKF estimated values of $\boldsymbol{\sigma_0}$ and $\boldsymbol{k_w}$, or $\boldsymbol{\psi}$, are the columns of $\overline{\Psi}_p$.

In summary, the EnKF is used to estimate the wake model parameters in the vector $\boldsymbol{\psi}$ for a given realization from the probability distribution of finite time averaged SCADA data $\widetilde{\boldsymbol{P}}$. The EnKF estimation is used to map the probability distribution of power production samples $f(\widetilde{\boldsymbol{P}})$ to the distribution of wake model parameters $f(\boldsymbol{\psi})$, which is required for the expected value calculation in Eq. (2). The wake model parameter distribution method proposed here neglects structural model form bias and uncertainty, which should be considered in future work.

III. UTILITY-SCALE WIND FARM CASE STUDY

The optimization under model parameter uncertainty will be analyzed for open-loop control using a utility-scale wind farm case study. In Sec. III A, field measurements from the utility-scale wind farm are used to inform the wind condition probability distributions in Eq. (2). The yaw misalignment set-point lookup table is synthesized in Sec. III B. Wake model-based numerical experiments are performed in Sec. III C. Since the same wake model is being used to construct and test the lookup table in these experiments, this can be viewed as an

to construct and test the lookup table in these experiments, this can be viewed as an idealized, perfect model setting to test the stochastic programming performance with no structural wake modeling error. In Sec. IV, the optimization framework is tested in closed-loop control in LES.

The wind farm is located in northwest India. The wind turbines have approximately 100 meter diameters and hub heights and the terrain is flat with no significant complexity. The rated power for the turbines is approximately 2 MW. Two clusters of turbines are considered as shown in Fig. 2. For cluster A, the flow of interest is centered at $\alpha \approx 0^{\circ}$, where 0° corresponds to north and proceeds clockwise, such that turbines $A3$ and $A4$ experience wake losses from turbine $A1$. For cluster B, the focus for wake steering is $\alpha \approx 270^{\circ}$, where turbines $B2$, $B3$, and $B4$ experience wake losses. One min averaged SCADA data are recorded from the wind farm.

FIG. 2. (a) Utility-scale wind farm layout for cluster A. The turbines are oriented for flow from the north ($\alpha = 0^{\circ}$) and the coordinates are normalized by the wind turbine diameter D. (b) Cluster B layout oriented for flow from the west ($\alpha = 270^{\circ}$). The wind turbine which is used as a wind condition reference is shown in red. The x and y axes correspond to easting and northing directions.

PPT | High-resolution

In open-loop control, there is a set of hyperparameters associated with the wind condition bin widths for the yaw set-point lookup table. Contemporary wind turbine control systems are computational operation count and memory limited, which restricts the quantity of wind condition bins in the lookup table. In the present study, we will use wind speed $u \pm 1$ m/s, wind direction $\alpha \pm 2.5^{\circ}$, and turbulence intensity $TI \pm 2.5\%$, which is based on the memory limitations of a utility-scale wind turbine control system and similar to previous studies.[4] The methods developed in this study apply to arbitrary wind condition lookup table selections, although the specific probability distributions for each wind condition may be changed with different bin width selections.

A. Probability distributions for wind conditions

In open-loop lookup table synthesis, given the finite width of the wind condition bins which is not infinitesimally small, there is a probability distribution associated with each wind condition within each bin. For example, for the freestream wind speed bin $5 < u < 7$ m/s, there will be a probability distribution associated with the wind speed values in this restricted range. The historical SCADA measurements for wind direction, speed, and yaw

misalignment will be used to define empirical probability distributions used in Eq. (2). The SCADA data can be used both to establish a likelihood for each wind condition bin in the lookup table and to establish wind condition probability distributions within each lookup table bin. The field data probability distributions for the wind direction and speed can be seen in Figs. 3(a) and 3(b). The wind direction within the wind condition bin can be approximated by a uniform distribution. As discussed thoroughly by Rott *et al.*[18] and Simley *et al.*,[19] there is uncertainty associated with the measurements of the wind direction as well as higher frequency dynamics which occur within a 1 min averaged sample that could cause larger values of α deviations. In order to account for these dynamics, we will consider α uncertainty of $\alpha \pm 2.5^\circ$, $\alpha \pm 5^\circ$, and $\alpha \pm 10^\circ$ in the case studies presented in Sec. III B. The case of $\alpha \pm 2.5^\circ$ corresponds to wind direction variability from the bin width, whereas higher uncertainty values of $\pm 5^\circ$ and $\pm 10^\circ$ consider other variability and uncertainty factors. Previous approaches considered higher frequency content and used Gaussian distributions to model directional variability.[18] In this open-loop experiment, we will focus on low-pass filtered wind condition variations within a lookup table bin since SCADA data were not available at higher frequency than 1 min averages. Higher frequency content will be considered in the LES case study in Sec. IV.

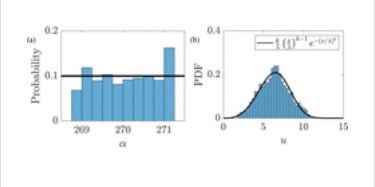

FIG. 3. (a) Wind direction probability distribution within a $268.75^\circ < \alpha < 271.25^\circ$ wind direction bin. (b) Wind speed empirical probability density function. A best-fit Weibull distribution with $k = 3.8$ and $\lambda = 7$ is shown with a solid black line.

PPT | High-resolution

The wind speed approximately follows a Weibull distribution [Fig. 3(b)]. The subset of the Weibull distribution corresponding to the wind speed bounds of the wind condition bin of interest is used to define the probability distribution of the wind speed in the bin. The Weibull is truncated to the interval of interest (e.g., between 5 and 7 m/s) and renormalized accordingly. The yaw error probability distribution for turbine $A1$ is shown in Fig. 4(a). A Gaussian probability density function is used to approximate the distribution with $\sigma_\gamma = 5.6^\circ$.

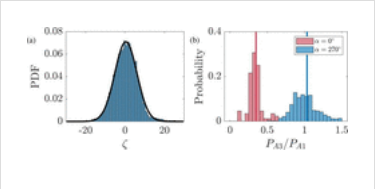

FIG. 4. (a) Yaw error ζ empirical probability density function with a best-fit Gaussian distribution shown with a solid black line. The mean and standard deviation of the Gaussian distribution are $\mu_\zeta = 0.4^\circ$ and $\sigma_\zeta = 5.6^\circ$. (b) Wind turbine power ratio probability distributions for wind direction bins centered at $\alpha = 0^\circ \pm 2.5^\circ$ and $\alpha = 270^\circ \pm 2.5^\circ$ for $u = 7 \pm 1$ m/s and $TI = 5\% \pm 2.5\%$. The vertical lines correspond to the means of the respective power ratio distributions.

B. Open-loop control yaw misalignment set-point lookup table synthesis

The wake model parameters are estimated using the normalized, 1 min averaged SCADA power production data, $\widetilde{P}/\widetilde{P}_1$, where $\widetilde{P}_1$ is the power of the leading, freestream operating turbine in the array. The wind turbine array power production data are sorted such that instances with wind conditions u, α, and TI are collated within a particular lookup table bin and matched with the corresponding 1 min averaged power productions. The power production empirical probability distributions for 1 min averaged $\widetilde{P}_{A3}/\widetilde{P}_{A1}$ for $\alpha = 0^\circ \pm 2.5^\circ$ and $\alpha = 270^\circ \pm 2.5^\circ$ are shown in Fig. 4(b). The wind speed is filtered such that $u = 7 \pm 1$ m/s and $TI = 5\% \pm 2.5\%$. For $\alpha = 270^\circ \pm 2.5^\circ$, turbine $A3$ does not experience waked incident inflow, and therefore, $\widetilde{P}_{A3}/\widetilde{P}_{A1} \approx 1$ with variations due to spatiotemporal differences in the ABL turbulent inflow in 1 min averaged samples. The resulting distribution for $\widetilde{P}_{A3}/\widetilde{P}_{A1}$ can be reasonably approximately by a Gaussian, centered around $\langle \widetilde{P}_{A3}/\widetilde{P}_{A1} \rangle \approx 1$. For $\alpha = 0^\circ \pm 2.5^\circ$, turbine $A3$ experiences significant wake losses, with $\langle \widetilde{P}_{A3}/\widetilde{P}_{A1} \rangle \approx 0.4$. However, within the narrow wind direction and speed bins, $\widetilde{P}_{A3}/\widetilde{P}_{A1}$ is still reasonably Gaussian.

The normalized power productions for turbine $B2$ are shown in Fig. 5 for $TI = 5 \pm 2.5\%$ and $TI = 10 \pm 5\%$. The wind speed is $u = 7 \pm 1$ m/s and various wind directions α are shown. For the wind farm layouts shown in Fig. 2, the peak wake losses occur at direct wind turbine alignment, which is approximately $\alpha = 260^\circ$ for turbine $B2$. The mean SCADA power production data are shown with error bars representing one standard deviation about the mean. The wake model parameters are estimated using the SCADA data. The resulting wake model power production estimation is shown in Fig. 5, where the blue triangles estimate the wake model parameters only based on the mean $\overline{P} = \langle \widetilde{P} \rangle$. For the parametric uncertainty (red), the wake model estimates the model parameters for the distribution of $\widetilde{P}$ for each wind direction bin. The wake model estimates parameters k_w and σ_0 to capture the various power production targets, including $\overline{P} \pm \sigma_p$, except for wind directions where wake losses do not occur, such as $\alpha < 250^\circ$ or $\alpha > 270^\circ$ for turbine $B2$. Wind directions such as $\alpha > 270^\circ$ for turbine $B2$ will not be relevant to the optimization in Eq. (2) since $\gamma^*_{s,B1} = 0^\circ$ from geometry. The model used in this study is only able to realize power production differences between the waked and freestream turbines which manifest from wake losses and cannot capture all variations which include effects from temporally dependent, stochastic, heterogeneous flow fields. The model cannot estimate $P_{B2} > P_{B1}$ which occurs in freestream operation for $\overline{P}_{B2} + \sigma_{p,B2}$ as a result of spatially and temporally varying ABL turbulence. Future work can incorporate spatiotemporal inflow variations[46] to more accurately model these effects. The expected values of the wake model parameters

estimated for cluster B are shown in Fig. 17 in Appendix A.

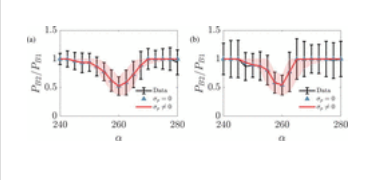

FIG. 5. Normalized power production for waked turbine *B*2 in cluster B as a function of the incident wind direction for $u = 7 \pm 1$ m/s and (a) $TI = 5 \pm 2.5\%$ and (b) $TI = 10 \pm 2.5\%$. Errorbars represent one standard deviation about the mean from the 1 min averaged SCADA data. The stochastic wake model predictions are represented by $\sigma_p \neq 0$. The shaded region corresponds to one standard deviation about the mean wake model power estimate.

PPT | High-resolution

The resulting optimal yaw misalignment angles $\boldsymbol{\gamma}_s^*$ from various variability and uncertainty cases are shown for turbine *B*1 in Fig. 6 for the two turbulence intensity cases. Positive yaw misalignment corresponds to a counterclockwise rotation viewed from above. The optimization cases with model parameter uncertainty are represented by $\boldsymbol{\sigma}_p \neq 0$. Cases with $\boldsymbol{\sigma}_p \neq 0$ optimize $\boldsymbol{\gamma}_s$ considering parametric uncertainty. The probability distribution of the model parameters $f(\boldsymbol{\psi})$ is discretized with nine points across the probability space in the numerical integration of Eq. (1), and the probability distribution is assumed to be Gaussian, as discussed in Sec. III B. For the lower turbulence intensity inflow [Fig. 6(a)] and deterministic yaw optimization, the yaw set-points have a sharp inflection point around $\alpha \approx 260^\circ$, where the sign of the optimal yaw switches. The yaw misalignment values for turbine *B*1 are not symmetric about the inflection point since the wind turbine array is not directly aligned [see Fig. 2(b)].

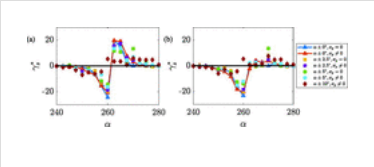

FIG. 6. Model-optimal yaw misalignment angles for turbine *B*1 as a function of the incident wind direction for $u = 7 \pm 1$ m/s and (a) $TI = 5 \pm 2.5\%$ and (b) $TI = 10 \pm 2.5\%$. Optimal yaw set-points for various wind direction uncertainties are shown. Cases with $\alpha \pm 0^\circ$ are deterministic set-point optimization with respect to the wind direction and $\sigma_p = 0$ are deterministic with respect to the wake model parameters. The optimization with model parameter uncertainty is represented by $\sigma_p \neq 0$ cases.

PPT | High-resolution

The influence of wind direction uncertainty on optimal set-point values has been characterized in previous studies.[16,18] Given uncertainty or variability in the wind direction, small changes in α as a function of time would result in suboptimal $\boldsymbol{\gamma}_s^*$ for instantaneous wind condition realizations. With increasing α uncertainty, the $\boldsymbol{\gamma}_s^*$ profile is generally smoothed around the inflection point. Wind direction uncertainty of $\alpha \pm 10^\circ$ results in

dramatic changes compared to deterministic set-point optimization, where $\gamma_s^*(\alpha = 260^\circ)$ becomes small and positive, instead of the deterministic negative value. This model-optimal value is the result of a balance of weighting power production for $\pm 10^\circ$ around the inflection point.

The normalized SCADA power and modeled power production for turbine $A3$, and associated optimal yaw angles for turbine $A1$, are shown in Figs. 7(a) and 7(b). For turbine $A3$, the maximum wake loss inflection point occurs at approximately $\alpha = -2.5^\circ$. For cluster A, the incorporation of α or $\boldsymbol{\sigma_p}$ uncertainty has a less pronounced impact on $\boldsymbol{\gamma}_s^*$ due to the tight spacing in the streamwise direction $(4 - 5D)$ and relatively small values of power production standard deviation within wind direction bins. The expected values of the wake model parameters of turbine $A1$, $\mathbb{E}(\boldsymbol{\psi}) = \int \boldsymbol{\psi}' f(\boldsymbol{\psi}') d\boldsymbol{\psi}'$, are shown in Fig. 8 for the stochastic and deterministic model parameter cases. The expected values of the model parameters are similar in the two cases due to the low magnitude of turbulence in test case A. In this case, the stochastic parameters have decreased the expected value of k_w and increased the expected value of σ_0. Since the two-parameter wake model is potentially over parameterized,[17] future work should investigate physics-based constraints for σ_0. Some presence of nonphysical wake model parameters exists in the estimated distributions ($k_w < 0$), which could be alleviated by tailoring the prior, using Bayesian sampling methods (e.g., MCMC) to more accurately estimate parameter posteriors, or by increasing the time-averaging length of the SCADA data. Future work should also investigate imposing physical constraints for the parameters in the estimation routine.

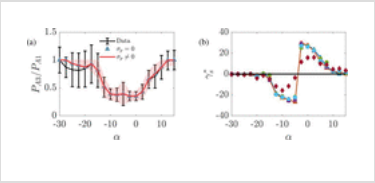

FIG. 7. (a) Normalized power production for waked turbine $A3$ in cluster A as a function of the incident wind direction for $u = 7 \pm 1$ m/s and $TI = 5 \pm 2.5\%$. Error bars represent one standard deviation about the mean from the 1 min averaged SCADA data. The shaded region corresponds to one standard deviation about the mean wake model power estimate. (b) Model-optimal yaw misalignment angles for turbine $A1$ given the power production distribution in (a). The symbols are identified in the legend of Fig. 6.

PPT | High-resolution

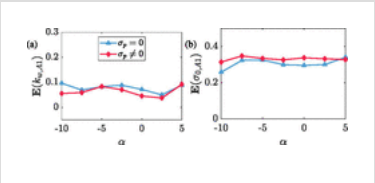

FIG. 8. The expected values of the model parameters for turbine $A1$ in cluster A as a function of the incident wind direction for $u = 7 \pm 1$ m/s and $TI = 5 \pm 2.5\%$ for (a) k_w and (b) σ_0. Estimates of the expected value of the wake model parameters based on the mean of the power data are given by $\sigma_p = 0$, which corresponds to a wake model with deterministic wake model parameters. The expected value of the model parameters considering uncertainty is shown with

$\sigma_p \neq 0$.

C. Wake model-based open-loop wake steering case studies

Several wake steering case studies are performed to examine the influence of the set-point optimization methodology. The wake model described in Sec. II A is used for the case studies. SCADA data are used to select instances of time such that the wind speed, direction, and turbulence intensity are within wind conditions of interest. The longest, continuous time series of such instances is selected for each test case (the length of the time series for each case is given in Table I and is between 30 and 144 min, depending on the case). The case study data differs from the training data which is used for optimal yaw set-point calculation, ensuring there is not a bias in using the same data for training and testing. Quality filters are used on the SCADA data to ensure all wind turbines of interest are operating normally with no curtailments or error codes. In the case study tests, the 1 min averaged SCADA data samples are provided to the wake model parameter estimation (Sec. II B), and the optimal parameters for the specific instances are computed which minimize the wake model fitting error. The yaw set-points are obtained from the precalculated lookup table (Sec. III B) and applied in the wake model, which models the power production given the computed optimal parameters, the 1 min averaged wind speed and direction, and the different yaw misalignment strategies for each 1 min instance. Yaw controllers for utility-scale turbines modify yaw with a speed around 0.5°/s. Large, 1 min changes in yaw misalignment ($\gamma_s > 30°$), which would not be feasible, occur less than 0.5% of the time in these case studies, and therefore, the yaw modifications were not restricted for controller simplicity. Since the case studies use 1 min averaged data, higher frequency variations in the power production, model parameters, and wind conditions are not included in this numerical experiment, and their influence is considered in LES (Sec. IV).

TABLE I.

Wake steering control numerical experiment power production results provided as a percent change with respect to baseline yaw-aligned control. Red and green cases have statistically significantly lower and higher power than $\alpha \pm 0.0°$, $\sigma_p = 0$, characterized by a two-sided two-sample Kolmogorov–Smirnov test at 5% significance level, respectively. Deterministic model parameter set-point optimization is represented by $\sigma_p = 0$. The number of 1 min averaged data points in the timeseries is given by n. (1) Cluster B, $u = 7 \pm 1$ m/s, $TI_u = 5 \pm 2.5\%, n = 73$; (2) Cluster B, $u = 7 \pm 2$ m/s, $TI_u = 5 \pm 5\%, n = 144$; (3) Cluster B, $u = 7 \pm 2$ m/s, $TI_u = 10 \pm 2.5\%, n = 51$; (4) Cluster B, $u = 9 \pm 2$ m/s, $TI_u = 10 \pm 2.5\%, n = 32$; (5) Cluster A, $u = 7 \pm 2$ m/s, $TI_u = 5 \pm 2.5\%, n = 115$.

Case					
Model uncertainty	**(1) (%)**	**(2) (%)**	**(3) (%)**	**(4) (%)**	**(5) (%)**
$\alpha \pm 0.0^{\circ},\ \sigma_p = 0$	2.3	2.2	0.4	−0.3	8.7
$\alpha \pm 0.0^{\circ},\ \sigma_p \neq 0$	3.8	2.3	0.0	−0.1	8.8
$\alpha \pm 10^{\circ},\ \sigma_p \neq 0$	0.5	1.3	−0.3	0.1	4.2

The results from five wake steering case studies are shown in Table I. For cluster B at a low incident turbulence intensity (case 1), deterministically optimized yaw set-point increases power 2.3%, while considering parameter uncertainty increases power 3.8% which is statistically significantly higher. Incorporating wind direction variability of $\pm 2.5^{\circ}$ does not significantly impact the results. The power production results for each optimization strategy in case 1 are shown in Fig. 9. Higher wind direction variabilities of $\pm 5^{\circ}$ or $\pm 10^{\circ}$ reduce the power significantly in this case by reducing the set-point optimal yaw angles (see Fig. 6). It is worth noting that these case studies only consider frequencies lower than $f_c = 1/60$ Hz due to 1 min averaging, while the wind conditions have higher frequency content.[18] The higher frequencies are included in the empirical wind condition probability distributions in Eq. (2) in the LES experiments in Sec. IV.

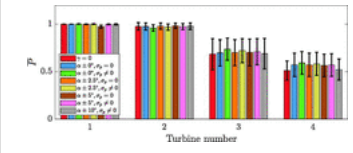

FIG. 9. Time-averaged power production results from case 1. The error bars denote one standard deviation about the mean values. The results of this case are summarized in Table I.

PPT | High-resolution

With increasing turbulence intensity, variability in the wind conditions and power production increases. For the higher turbulence intensity cases, the power increase due to wake steering decreases, which is expected due to the increased mixing and reduced wake interactions. With higher turbulence intensity in cases 3 and 4, the power increase due to wake steering is diminished and the different optimization methods are generally not significantly different in their performance. Incorporation of variability in the set-point optimization does not significantly influence cluster A results in case 5, except for $\alpha \pm 10^{\circ}$, which produces significantly less power than the other cases. The relatively small impact of parameter uncertainty in cluster A is likely due to the small spacing between turbines, low turbulence intensity inflow, and low power production standard deviation (Fig. 7).

In summary, the wake model experiments in this section demonstrate the utility of the yaw set-point optimization under parameter uncertainty approach in an idealized numerical setting with no structural modeling error. These results also demonstrate that the incorporation of wake model parameter uncertainty in stochastic programming reduces the sensitivity of the optimal set-points $\boldsymbol{\gamma}_s^*$ to overfitting to the training data. In the time series numerical experiments, the wind conditions and temporally local wake model parameters in the wake model vary. The deterministic wake model only produces a single set of wake model parameters based on the training data to optimize $\boldsymbol{\gamma}_s$ in the lookup table. In these numerical examples, the wake steering test results are improved, at low turbulence intensity, when considering a distribution of wake model parameters from the training data, rather than deterministic parameters, even in the presence of some unphysical wake model parameters in the parameter distributions. The more realistic application including modeling error is described in the LES experiments in Sec. IV. Future work should investigate the physical bounds for wake model parameters in the representation of finite time averaged wakes.

IV. LARGE EDDY SIMULATIONS OF CLOSED-LOOP CONTROL IN AN UNSTABLE BOUNDARY LAYER

In this section, large eddy simulations of a nine turbine model wind farm are performed in unstable, convective ABL conditions using closed-loop wake steering control. The primary goal of this section is to investigate the impact of incorporating uncertainty in the yaw set-point optimization on the closed-loop wake steering control approach for different selections of control update timescales. In these numerical experiments, the LES wind farm will represent a utility-scale wind farm which is using closed-loop wake steering control to increase power as a function of time in the transient, unstable ABL. An unstable ABL test case was selected, instead of the standard, idealized neutral[27] or conventionally neutral ABL,[17] due to its inherent wind condition variability and its prevalence in a utility-scale wind farm setting, occurring during daytime operation. The wake model will be used for yaw set-point optimization, as in Sec. II. Therefore, this case represents a more realistic numerical experiment where wake modeling error is present, such that the wake model does not resolve all physical phenomena in the LES wind farm. The LES and closed-loop control setup

resolve all physical phenomena in the LES wind farm. The LES and closed-loop control setup are described in Sec. IV A and the results are presented in Sec. IV B.

A. LES and closed-loop control setup

Large eddy simulations are performed using the open-source pseudospectral code *PadéOps* (https://github.com/FPAL-Stanford-University/PadeOps). The code has previously been used for a variety of LES studies including modeling turbulence in the planetary boundary layer,[47] Coriolis effects in the ABL,[48–50] and multirotor turbines.[51] *PadéOps* has also been used to perform closed-loop wake steering simulations in the conventionally neutral ABL.[17,31] Full details of the numerical setup are given in Ghate and Lele[47] and Howland *et al.*,[17] and key details are restated here for completeness.

The flow is forced using a geostrophic pressure gradient corresponding to a geostrophic wind speed magnitude $G = 8$ m/s. The geostrophic wind direction is westerly, aligning with the x-axis in the computational domain. Coriolis effects are included with the traditional approximation enforced[49] to enable a validation of the convective ABL case with reference LES data from the literature.[52] Wind turbines are represented by the actuator disk model[53] described by Howland *et al.*[17] The wind turbines have a hub height of 100 m and a diameter of $D = 126$ m. The cosine factor for C_p is set to the conservative value of $P_p = 2.5$ since underestimates of P_p significantly degrade wake steering performance.[17]

An unstable, convective ABL is simulated using LES. The domain is $12 \times 4 \times 2$ km^3 with 480, 320, and 320 grid points in the x, y, and z directions, respectively. The Rossby number based on the initial boundary layer height of $\delta = 1$ km and the geostrophic wind speed is $Ro = 110$ and the Froude number is $Fr = 0.08$. The concurrent precursor methodology is used.[54] Fringe regions to force the primary simulation to the precursor inflow are used in the last 25% of the computational domain to ensure no upstream contamination of the solution in the region of interest due to the fringe.[50,55] A sponge region is used in the top 25% of the vertical direction.[17] The ABL is initialized with $u = G$, and all other velocity is zero, and the potential temperature θ profile provided in Fig. 11(a). The surface heat flux is prescribed as $\langle w'\theta' \rangle = 0.1$ K m/s, corresponding to unstable ABL conditions. The simulation is run for 1 h to remove startup transience. The wind farm layout in the primary domain is shown in Fig. 10. The turbines of interest are 1–8 and turbine R is used as a yaw-aligned reference turbine in all cases.

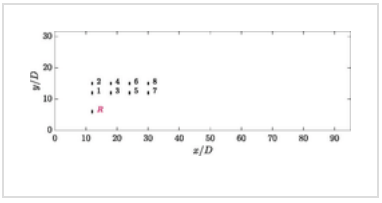

FIG. 10. LES wind farm layout with the coordinates normalized by the wind turbine diameter. The geostrophic wind direction is in the *x* direction. Turbine *R*, shown in red, is the reference turbine and is yaw-aligned in all LES cases.

PPT | High-resolution

Within the convective, unstable ABL, three separate yaw set-point optimization cases are run in addition to baseline, yaw-aligned control. For baseline, yaw-aligned control, the wind turbines in the wind farm update their nacelle orientation according to a predefined control update period T. The nacelle position is updated to the value of the turbine specific mean wind direction measured during the previous finite time average horizon corresponding to the control update period, i.e., at time t, the nacelle position is set to equal $\alpha_T = \frac{1}{T}\int_{t-T}^{t} \alpha(t')\mathrm{d}t'$. While more sophisticated controllers could be implemented (e.g., the yaw control acts if the moving average of instantaneous yaw exceeds a deadband threshold) this approximate yaw alignment controller is used as a representative baseline, yaw-aligned control case.

For the wake steering cases, the closed-loop control developed in Howland *et al.*[17] is used, and is briefly described here for completeness. Using the same control update period as the baseline, yaw-aligned control, the nacelle position is updated according to the mean wind direction measured by each turbine plus an additional yaw misalignment offset corresponding to the set-point optimization result $\alpha_{T,i} + \gamma^*_{s,i}$, for turbine i. The yaw misalignment set-point is optimized differently in three distinct cases. In deterministic set-point optimization, the mean wind conditions over the previous control update period measurements are used to optimize the deterministic wake model, with no variability or uncertainty in the wind conditions or wake model parameters. For the stochastic wind conditions case, the stochastic programming formulation in Eq. (1) is used for variable wind conditions but for deterministic wake model parameters. The wind condition probability distributions are constructed using the measurements collected over the previous control update window $t - T \rightarrow t$. The wake model parameters are fit using the standard EnKF, using the mean power production to produce only one set of wake model parameters. Finally, the full stochastic programming framework is used where the variable wind conditions are used in addition to the uncertain wake model parameter methodology described in Sec. II. Each of the four cases, the single yaw-aligned case and the three wake steering cases, represents a separate LES simulation. In all cases, the reference turbine R uses yaw-aligned control throughout the simulation.

The four simulations are run for three different control update periods of T = 12.5, 18.75, and 25 min. The performance of wake steering in transient flow depends on the frequency of the controller update; with shorter control update periods the yaw controller can react to high-frequency variations in the wind conditions.[28] However, following the central limit theorem, for reduced control update periods T, there will be increased variability and uncertainty in the finite time averaged quantities, such as power production, which are used to inform the set-point optimization. Conversely, for longer update periods, the mean flow state may evolve, as can be seen in the wind direction in Fig. 11(b), for example. The implications of the length of T on finite time averaged statistics, such as α_T, is shown in Figs. 11(b) and 11(c), for

T = 12.5 and 25 min. While future work should investigate the optimal update period T as a function of the ABL flow state, in this study, we present results for selected, predefined values of T.

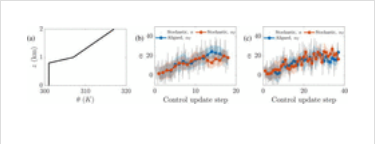

FIG. 11. (a) Unstable LES initial potential temperature profile θ as a function of height z. (b) Unstable LES wind direction as measured by the reference turbine R (Fig. 10). The finite time averaged wind direction α_T with T = 25 min is shown as a function of the control update steps for the aligned and optimization under uncertainty (stochastic) LES cases. The shaded regions correspond to one standard deviation around the mean. The instantaneous wind direction for the optimization under uncertainty LES case is shown as α. (c) Same as (b) for T = 12.5 min.

PPT | High-resolution

B. LES results

Within the convective ABL, there is a high magnitude of turbulence intensity and wind condition variability, compared to the standard neutral or conventionally neutral test cases which have previously been used for closed-loop control numerical experiments.[17] The streamwise turbulence intensity at the wind turbine hub height is approximately $TI = 15\%$, although the specific value changes during the transient simulation. An instantaneous visualization of the streamwise velocity flow field at the wind turbine hub height is shown in Fig. 12 for the yaw-aligned case after the first yaw control update. In general, convective ABL conditions produce less significant wake interactions between wind turbines compared to neutral or stable states of stratification[56] due to high turbulence intensity and convective plumes with large length scales.

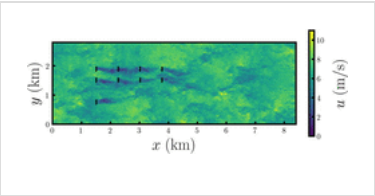

FIG. 12. Instantaneous streamwise velocity u flow field at the wind turbine hub height for the yaw-aligned case.

PPT | High-resolution

The wind directions measured by the yaw-aligned reference turbine in the stochastic conditions and parameters simulation and the aligned simulation are shown in Fig. 11(b) for T = 25 min and Fig. 11(c) for T = 12.5 min. The mean wind directions averaged over the control update step are shown in addition to the instantaneous wind direction measurements. The two cases are initialized from identical states, but the wind direction measurements diverge

two cases are initialized from identical states, but the wind direction measurements diverge due to the chaotic nature of turbulent flow. For all control update steps, the mean wind direction measurements are within one standard deviation of one another, but the magnitude of the variations in the instantaneous wind direction data are significant. Given the exponential divergence of the states in the chaotic flow and the high magnitude of variability in the convective ABL, integrated energy measures will be used to characterize the performance of each case. The integral time scales of the reference turbine power and wind direction measurements are approximately 60 and 90 s, respectively.

The yaw misalignment set-points as a function of time for the control update period of T = 12.5 min are shown in Fig. 13 for turbines 1, 3, and 5. The deterministic yaw set-point optimization exhibits significant variability in the set-point value as a function of the control update step. The deterministic set-point optimization is sensitive to uncertainty in the limited time-averaged statistics, since the yaw misalignment decision is based on the singular valued mean wind conditions and wake model parameters which are subject to the internal variability of the ABL flow [e.g., the averaged wind direction α_T will have more inherent variability for T = 12.5 min than T = 25 min as shown in Fig. 11(c)]. Therefore, between control update steps, the finite time averaged statistics may change dramatically, resulting in significant changes in $\boldsymbol{\gamma}_s^*$.

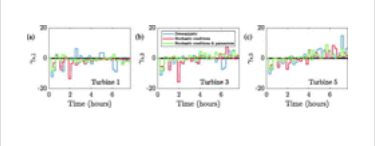

FIG. 13. Yaw misalignment set-points as a function of time for T = 12.5 min for turbines (a) 1, (b) 3, and (c) 5. The yaw misalignment set-points are shown relative to the local wind direction at each wind turbine.

PPT | High-resolution

The yaw misalignment set-points for the stochastic programming considering wind condition variability but with deterministic wake model parameters are also shown in Fig. 13 for T = 12.5 min. The incorporation of the stochastic wind conditions in the optimization reduced the magnitude of the yaw misalignment values and the variability of the yaw values between control update steps. Comparing the optimization with and without parameter uncertainty demonstrates that incorporating the parameter uncertainty mitigates the variations $\boldsymbol{\gamma}_s^*$ as a function of the control update steps. Provided with limited information in the finite time average over length T, the optimization under parameter uncertainty also suppresses overfitting to the mean power production values.

The yaw set-points for T = 18.75 min are shown in Figs. 14 and 15. The yaw misalignment values for all eight turbines in the LES for T = 18.75 are shown individually in Appendix B. For the T = 25 min simulations, the yaw set-points are shown in Fig. 16. The set-point variability results are similar to T = 12.5 and T = 18.75 min. However, contrarily to T = 12.5 min, the stochastic conditions and parameters case resulted in the largest absolute value of yaw misalignment with T = 25 min. With a larger T, the states recorded over the time window

misalignment with $T = 25$ min. With a larger T, the states recorded over the time window $t - T \rightarrow t$ used to inform the yaw set-point optimization at time t have a larger variability. Depending on the joint distributions of the wind conditions and wake model parameters, the optimization under parameter uncertainty may result in larger absolute values of yaw misalignment set-points due to their nonlinear influence on wind farm power production in the wake model. In this particular numerical example, this occurred for $T = 25$ min, but not for $T = 12.5$ min, indicating the complex relationship between the wind conditions and wake model parameters and the optimal yaw set-points.

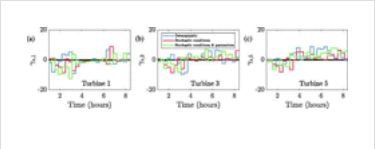

FIG. 14. Yaw misalignment set-points as a function of time for $T = 18.75$ min for turbines (a) 1, (b) 3, and (c) 5. The yaw misalignment set-points are shown relative to the local wind direction at each wind turbine.

PPT | High-resolution

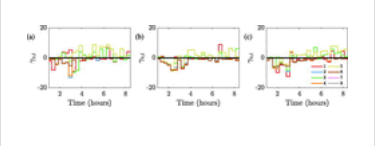

FIG. 15. Yaw misalignment set-points as a function of time for $T = 18.75$ min. (a) Deterministic yaw set-point optimization, (b) yaw set-point optimization with variable wind conditions, and (c) yaw set-point optimization with variable wind conditions and uncertain wake model parameters. The yaw misalignment set-points are shown relative to the local wind direction at each wind turbine.

PPT | High-resolution

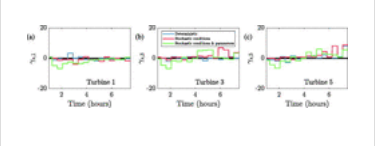

FIG. 16. Yaw misalignment set-points as a function of time for $T = 25$ min for turbines (a) 1, (b) 3, and (c) 5. The yaw misalignment set-points are shown relative to the local wind direction at each wind turbine.

PPT | High-resolution

As shown qualitatively in Figs. 13, 14, and 16, the closed-loop control strategy with deterministic optimization is sensitive to the control update period. In closed-loop control, the yaw misalignment angles are selected based on the optimization of the wake model [Eq. (1)], based on the finite time averages of the wind conditions and the estimated model parameters. In the closed-loop control, there is an inherent trade-off in the yaw update frequency.[28] A higher update frequency enables the wind farm to react to local wind condition information but introduces noise into the wind condition and power

measurements, which affect the model-optimal yaw misalignment angles. We anticipate that the incorporation of wind condition and model parameter uncertainty in the stochastic programming problem will reduce the sensitivity of the wake steering control strategy to the yaw misalignment update period, compared to optimization with deterministic wind conditions and model parameters.

The sensitivity of the yaw misalignment set-point values to the control update period is tested by comparing the set-points for different update period selections with fixed optimization methods. For example, the yaw set-points for deterministic optimization will be compared for $T = 12.5$ and $T = 18.75$ min. The different simulations are run over the same physical time window of $T_f \approx 9$ h. The lower control update periods result in more frequent yaw updates. For comparison, the larger control update period yaw set-points are linearly interpolated to match the discrete instances of set-points for the more frequent yaw update case. The upsampled low-frequency set-points are denoted by $\widetilde{\boldsymbol{\gamma}}_s$. The resulting discrepancy between the two different control update periods is denoted by a mean squared deviation,

$$\Delta\gamma_s = \frac{1}{N_t}\sum_{i=1}^{N_t}\overline{(\gamma_{s,T_{\text{low},i}} - \widetilde{\gamma}_{s,T_{\text{high},i}})^2}, \tag{14}$$

where $\bar{\cdot}$ denotes the time average. Turbines 1–6 are considered in the summation. The reference turbine and turbines 7 and 8 are not considered since their yaw set-points are zero for all cases and for all times. The results are shown in Table II. Considering uncertainty in the wind conditions and wake model parameters reduced the sensitivity of the wake steering approach to decreases in T.

TABLE II.

Mean squared deviations between the yaw misalignment set-points $\boldsymbol{\gamma}_s$ for cases with different update period settings and fixed optimization methodology. The lower frequency (larger update period) set-point values are linearly interpolated to match the higher frequency in the comparison (denoted $\widetilde{\boldsymbol{\gamma}}_s$). The mean squared deviation $\Delta\gamma_s$ is computed using Eq. (14).

	Case		
Yaw update periods	**Deterministic**	**Stochastic conditions**	**Stochastic conditions and parameters**
$\overline{(\boldsymbol{\gamma}_{s,12.5\,\text{min}} - \widetilde{\boldsymbol{\gamma}}_{s,18.75\,\text{min}})^2}$	11.8	8.7	6.9
$\overline{(\boldsymbol{\gamma}_{s,18.75\,\text{min}} - \widetilde{\boldsymbol{\gamma}}_{s,25\,\text{min}})^2}$	13.9	8.5	7.8
$\overline{(\boldsymbol{\gamma}_{s,12.5\,\text{min}} - \widetilde{\boldsymbol{\gamma}}_{s,25\,\text{min}})^2}$	12.2	9.9	8.0

The performance of each case is characterized using an integrated energy ratio,

$$E_r = \frac{\sum_{i=1}^{N_t} \int_0^{T_f} P_i(t)\mathrm{d}t}{N_t \int_0^{T_f} P^{ref}(t)\mathrm{d}t}, \tag{15}$$

which quantifies the wind farm performance compared to the reference turbine P^{ref} (turbine R, Fig. 10). The energy ratio E_r is, in practice, bounded by the limits [0, 1], where 0 corresponds to the wind farm turbines producing zero power and 1 indicating zero wake losses in the wind farm on average. The energy ratio metrics are integrated for approximately T_f = 9 h of physical wind farm operation; T_f is fixed for all cases.

The E_r results are shown in Table III. Confidence intervals are constructed for each case using bootstrapping. Given the large natural variation in this unstable ABL, the impact of wake steering on wind farm power production is not expected to be statistically significant. With T = 12.5 min, the stochastic conditions and stochastic conditions and parameters optimization cases marginally improve mean power compared to aligned control and deterministic optimization-based control, but the differences are not significant. For T = 25 min, the stochastic conditions only optimization has a mean E_r much lower than aligned control and deterministic optimization results in the highest mean E_r. The stochastic parameters and conditions optimization case slightly underperforms aligned control. An ensemble average is taken over the simulation results with different values of T. Overall, the optimization under model parameter and wind condition uncertainty had the highest E_r, followed by the aligned control (no wake steering) case. Wake steering with set-points optimized under wind condition uncertainty without parameter uncertainty resulted in a lower ensemble E_r than aligned control. Deterministic optimization had the lowest ensemble E_r, since the deterministic set-point optimization was sensitive to reductions in T.

TABLE III.

Unstable ABL LES closed-loop wake steering energy ratio E_r [Eq. (15)] results. The ensemble averages of the results over the different yaw update periods for fixed optimization methodologies are shown. The 95% confidence intervals, estimated by bootstrapping, are shown in parentheses.

	Case			
Yaw update period (min)	**Aligned**	**Deterministic**	**Stochastic conditions**	**Stochastic conditions and parameters**
T=12.5	0.84 (0.80, 0.89)	0.84 (0.79, 0.89)	0.86 (0.82, 0.92)	0.86 (0.81, 0.92)

$T=18.75$	0.84 (0.78, 0.91)	0.82 (0.76, 0.90)	0.86 (0.81, 0.92)	0.84 (0.78, 0.90)
$T=25$	0.86 (0.80, 0.94)	0.87 (0.80, 0.94)	0.82 (0.76, 0.88)	0.85 (0.79, 0.91)
Average	0.849	0.845	0.848	0.851

In summary, while the closed-loop wake steering control in unstable ABL conditions did not demonstrate statistically significant differences in wind farm energy production, the results demonstrate that the incorporation of stochastic wind conditions and wake model parameters in the yaw set-point optimization reduces the sensitivity of the wake steering approach to the control update and statistics integration length T. The ensemble average of energy ratios for the three control update period simulations was highest for the optimization under parameter uncertainty.

V. CONCLUSIONS

This paper extends yaw misalignment set-point optimization to include model parameter uncertainty. Previous studies have extended deterministic yaw set-point optimization to consider variability in the wind turbine yaw misalignment and incident wind direction. Wake model parameters are inherently variable and uncertain. The approach described in this paper optimizes the yaw misalignment set-points for wake steering over a probability distribution of wake model parameters. The optimization framework also incorporates wind speed and direction, yaw misalignment, and turbulence intensity variability. In this paper, due to the computational cost of Bayesian uncertainty quantification and the requirement for efficiency in closed-loop control, a simple, inexact estimate for the probability distribution of the model parameters is used.

The optimization under parametric uncertainty framework is implemented in open-loop wake steering wake model-based case studies where the incorporation of variability in the wake model parameters and the wind direction has a statistically significant impact on the power production in cluster B (moderate turbine spacing) at low turbulence intensity, but not in cluster A (tight turbine spacing) at low turbulence intensity or cluster B at high turbulence intensity. Notably, considering uncertainty in both wind conditions and wake model parameters in the set-point optimization had a statistically significantly higher power production than considering wind condition uncertainty alone.

The optimization under the parametric uncertainty framework is also tested in closed-loop wake steering control of a nine wind turbine wind farm in large eddy simulations of convective atmospheric boundary layer conditions. The optimization under the parametric uncertainty framework reduced the sensitivity of the closed-loop wake steering controller

to the yaw misalignment update period and reduced the variability in the yaw misalignment set-points as a function of the control update steps. However, incorporating parametric uncertainty did not have a statistically significant impact on the wind farm energy production due to the underlying variability in the power production in the convective boundary layer; notably, none of the wake steering cases had a significant power impact due to the wide the confidence intervals associated with the baseline yaw-aligned control efficiency.

The potential for wake steering to increase wind farm power depends on the ambient stratification.[4] It is anticipated that stable ABL conditions will have more potential for wake steering to increase power, compared to convective ABL conditions, with all else fixed at a wind farm. The closed-loop LES case studies presented in this study focused on the convective ABL with transient conditions to present a wake steering scenario with high turbulence intensity. Such conditions are relevant to the practical application of wake steering control since field conditions often exhibit higher variability than neutrally stratified LES case studies due to stratification[52] and large-scale variations in the atmosphere.[57] Unstable ABL conditions have also been encountered in initial field experiments of wake steering control.[4,37] Future work should investigate the impact of model parameter uncertainty in other stratification regimes. Since the model parameter uncertainty results, in part, from the variability in the wind flow and resulting farm power, it is anticipated that the parametric uncertainty in stable ABL conditions will be less significant.

The numerical experiments in this study demonstrate empirical benefits to incorporating parametric uncertainty in yaw set-point optimization, even with an inexact parameter distribution estimate method. Future work should consider sampling methods, such as MCMC,[25] to approximate the Bayesian posterior distribution used in the stochastic programming framework. This may require methodologies to speed up posterior sampling for application in closed-loop control, which requires efficient computation. Recent proposals, such as emulation-based sampling[58] or ensemble Kalman sampling,[59] may reduce the computational expense of the posterior estimation. Future work should also investigate the joint-probability distributions of the various parameters of interest in the wake steering problem. While this study used analytic gradient-based optimization, future work should more thoroughly compare the various yaw set-point optimization methodologies in use in the literature. Finally, future work should consider model bias in the form of structural model form uncertainty and its influence on the model parameter distributions and, more generally, on model-based set-point optimization.

ACKNOWLEDGMENTS

The author would like to thank John Dabiri, Aditya Ghate, and Carl Shapiro for thoughtful comments on the work and the manuscript. All simulations were performed on Stampede2 supercomputer under the XSEDE Project No. ATM170028. M.F.H. acknowledges partial

support from Siemens Gamesa Renewable Energy.

APPENDIX A: WAKE MODEL PARAMETERS FOR THE OPEN-LOOP WAKE STEERING NUMERICAL EXPERIMENTS

The expected value of the wake model parameters is shown in Fig. 17 for cluster B, turbine *B*3. The expected value is shown for the stochastic and deterministic model parameter cases. For low turbulence intensity [Figs. 17(a) and 17(b)], the expected value of the model parameters are similar in both cases due to the diminished variability. Larger differences arise between the cases at higher turbulence intensity. The relatively large variations in the wake model parameters are likely the result of the joint parameter estimation and due to the linear wake superposition used in the open-loop control numerical experiments. The wake superposition impacts the parameter estimates through a modification of the modeling error.[31] The improved modified linear superposition[20,31] is used in the LES case studies.

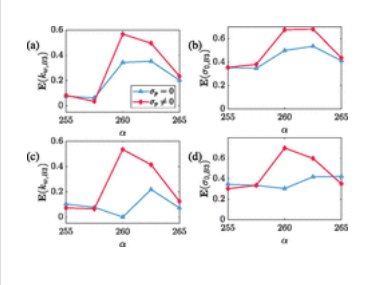

FIG. 17. The expected values of the model parameters for turbine *B*3 in cluster B as a function of the incident wind direction for $u = 7 \pm 1$ m/s and $TI = 5 \pm 2.5\%$ for (a) k_w and (b) σ_0 and for $u = 7 \pm 1$ m/s and $TI = 10 \pm 2.5\%$ for (c) k_w and (d) σ_0. Estimates of the expected value of the wake model parameters based on the mean of the power data are given by $\sigma_p = 0$, which corresponds to a wake model with deterministic wake model parameters. The expected value of the model parameters considering uncertainty is shown with $\sigma_p \neq 0$.

PPT | High-resolution

APPENDIX B: CONVECTIVE LES WIND FARM YAW MISALIGNMENT

The yaw misalignment values for all eight turbines considered in the unstable ABL LES closed-loop control experiments (Sec. IV) for the $T = 18.75$ min case are shown in Fig. 18.

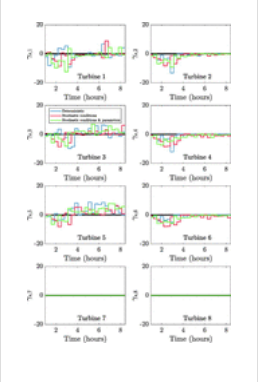

FIG. 18. Yaw misalignment set-points as a function of time for $T = 18.75$ min for all turbines in the LES model wind farm. The turbine layout and labels are provided in Fig. 10. The yaw misalignment set-points are shown relative to the local wind direction at each wind turbine.

PPT | High-resolution

DATA AVAILABILITY

The large eddy simulation data used in this study are available from the corresponding author on reasonable request. The utility-scale wind farm SCADA data are confidential at the request of the operator.

REFERENCES

1. M. F. Howland, J. Bossuyt, L. A. Martínez-Tossas, J. Meyers, and C. Meneveau, " Wake structure in actuator disk models of wind turbines in yaw under uniform inflow conditions," J. Renewable Sustainable Energy **8**, 043301 (2016). https://doi.org/10.1063/1.4955091, **Google Scholar**, **Scitation**, **ISI**

2. P. Gebraad, F. Teeuwisse, J. Van Wingerden, P. A. Fleming, S. Ruben, J. Marden, and L. Pao, " Wind plant power optimization through yaw control using a parametric model for wake effects–A CFD simulation study," Wind Energy **19**, 95–114 (2016). https://doi.org/10.1002/we.1822, **Google Scholar**, **Crossref**

3. P. Fleming, J. Annoni, J. J. Shah, L. Wang, S. Ananthan, Z. Zhang, K. Hutchings, P. Wang, W. Chen, and L. Chen, " Field test of wake steering at an offshore wind farm," Wind Energy Sci. **2**, 229–239 (2017). https://doi.org/10.5194/wes-2-229-2017, **Google Scholar**, **Crossref**

4. P. Fleming, J. King, K. Dykes, E. Simley, J. Roadman, A. Scholbrock, P. Murphy, J. K. Lundquist, P. Moriarty, K. Fleming *et al.*, " Initial results from a field campaign of wake steering applied at a commercial wind farm–Part 1," Wind Energy Sci. **4**, 273 (2019). https://doi.org/10.5194/wes-4-273-2019, **Google Scholar**, **Crossref**

5. M. F. Howland, S. K. Lele, and J. O. Dabiri, " Wind farm power optimization through wake steering," Proc. Natl. Acad. Sci. U. S. A. **116**, 14495–14500 (2019). https://doi.org/10.1073/pnas.1903680116, **Google Scholar**, **Crossref**

6. B. M. Doekemeijer, S. Kern, S. Maturu, S. Kanev, B. Salbert, J. Schreiber, F. Campagnolo, C. L. Bottasso, S. Schuler, F. Wilts *et*

Schreiber, F. Campagnolo, C. L. Bottasso, S. Schuler, P. Wilts *et al.*, " Field experiment for open-loop yaw-based wake steering at a commercial onshore wind farm in Italy," Wind Energy Sci. **6**, 159–176 (2021). https://doi.org/10.5194/wes-6-159-2021, **Google Scholar**, **Crossref**

7. J. van Wingerden, P. Fleming, T. Göçmen, I. Eguinoa, B. Doekemeijer, K. Dykes, M. Lawson, E. Simley, J. King, D. Astrain *et al.*, " Expert elicitation on wind farm control," arXiv:2006.07598 (2020). **Google Scholar**

8. J. C. Wyngaard, *Turbulence in the Atmosphere* (Cambridge University Press, 2010). **Google Scholar**, **Crossref**

9. J. Quick, J. Annoni, R. King, K. Dykes, P. Fleming, and A. Ning, " Optimization under uncertainty for wake steering strategies," J. Phys.: Conf. Ser. **854**, 012036 (2017). https://doi.org/10.1088/1742-6596/854/1/012036, **Google Scholar**, **Crossref**

10. F. Campagnolo, R. Weber, J. Schreiber, and C. L. Bottasso, " Wind tunnel testing of wake steering with dynamic wind direction changes," Wind Energy Sci. **5**, 1273–1295 (2020). https://doi.org/10.5194/wes-5-1273-2020, **Google Scholar**, **Crossref**

11. K. Johnson, L. J. Fingersh, and A. Wright, " Controls advanced research turbine: Lessons learned during advanced controls testing," Technical Report No. NREL/TP-500-38130, National Renewable Energy Laboratory, Golden, CO, 2005. **Google Scholar**, **Crossref**

12. P. Fleming, A. Scholbrock, A. Jehu, S. Davoust, E. Osler, A. D. Wright, and A. Clifton, " Field-test results using a nacelle-mounted lidar for improving wind turbine power capture by reducing yaw misalignment," J. Phys.: Conf. Ser. **524**, 012002 (2014). https://doi.org/10.1088/1742-6596/524/1/012002, **Google Scholar**, **Crossref**

13. J. R. Marden, S. D. Ruben, and L. Y. Pao, " A model-free approach

to wind farm control using game theoretic methods," IEEE Trans. Control Syst. Technol. **21**, 1207–1214 (2013). https://doi.org/10.1109/TCST.2013.2257780, **Google Scholar**, **Crossref**

14. J. Annoni, C. Bay, T. Taylor, L. Pao, P. Fleming, and K. Johnson, " Efficient optimization of large wind farms for real-time control," in *2018 Annual American Control Conference (ACC)* (IEEE, 2018). **Google Scholar**, **Crossref**

15. B. M. Adams, W. J. Bohnhoff, K. Dalbey, J. Eddy, M. Eldred, D. Gay, K. Haskell, P. D. Hough, and L. P. Swiler, " Dakota, a multilevel parallel object-oriented framework for design optimization, parameter estimation, uncertainty quantification, and sensitivity analysis: Version 5.0 user's manual," Sandia National Laboratories, Technical Report No. SAND2010-2183, 2009. **Google Scholar**

16. J. Quick, J. King, R. N. King, P. E. Hamlington, and K. Dykes, " Wake steering optimization under uncertainty," Wind Energy Sci. **5**, 413–426 (2020). https://doi.org/10.5194/wes-5-413-2020, **Google Scholar**, **Crossref**

17. M. F. Howland, A. S. Ghate, S. K. Lele, and J. O. Dabiri, " Optimal closed-loop wake steering–Part 1: Conventionally neutral atmospheric boundary layer conditions," Wind Energy Sci. **5**, 1315–1338 (2020). https://doi.org/10.5194/wes-5-1315-2020, **Google Scholar**, **Crossref**

18. A. Rott, B. Doekemeijer, J. K. Seifert, J-W v Wingerden, and M. Kühn, " Robust active wake control in consideration of wind direction variability and uncertainty," Wind Energy Sci. **3**, 869–882 (2018). https://doi.org/10.5194/wes-3-869-2018, **Google Scholar**, **Crossref**

19. E. Simley, P. Fleming, and J. King, " Design and analysis of a wake steering controller with wind direction variability," Wind Energy Sci. **5**, 451–468 (2020). https://doi.org/10.5194/wes-5-451-2020, **Google Scholar**, **Crossref**

20. A. Niayifar and F. Porté-Agel, " Analytical modeling of wind farms: A new approach for power prediction," Energies **9**, 741 (2016). https://doi.org/10.3390/en9090741, **Google Scholar**, **Crossref**

21. L. Zhan, S. Letizia, and G. V. Iungo, " Optimal tuning of engineering wake models through lidar measurements," Wind Energy Sci. **5**, 1601–1622 (2020). https://doi.org/10.5194/wes-5-1601-2020, **Google Scholar**, **Crossref**

22. B. M. Doekemeijer, J.-W. Van Wingerden, and P. A. Fleming, " A tutorial on the synthesis and validation of a closed-loop wind farm controller using a steady-state surrogate model," in *2019 American Control Conference (ACC)* (IEEE, 2019), pp. 2825–2836. **Google Scholar**, **Crossref**

23. J. Teng and C. D. Markfort, " A calibration procedure for an analytical wake model using wind farm operational data," Energies **13**, 3537 (2020). https://doi.org/10.3390/en13143537, **Google Scholar**, **Crossref**

24. M. F. Howland and J. O. Dabiri, " Wind farm modeling with interpretable physics-informed machine learning," Energies **12**, 2716 (2019). https://doi.org/10.3390/en12142716, **Google Scholar**, **Crossref**

25. J. Zhang and X. Zhao, " Quantification of parameter uncertainty in wind farm wake modeling," Energy **196**, 117065 (2020). https://doi.org/10.1016/j.energy.2020.117065, **Google Scholar**, **Crossref**

26. J. Schreiber, C. L. Bottasso, B. Salbert, and F. Campagnolo, " Improving wind farm flow models by learning from operational data," Wind Energy Sci. **5**, 647–673 (2020). https://doi.org/10.5194/wes-5-647-2020, **Google Scholar**, **Crossref**

27. B. M. Doekemeijer, D. van der Hoek, and J.-W. van Wingerden, " Closed-loop model-based wind farm control using FLORIS under

time-varying inflow conditions," Renewable Energy **156**, 719–730 (2020). https://doi.org/10.1016/j.renene.2020.04.007, **Google Scholar**, **Crossref**

28. S. Kanev, " Dynamic wake steering and its impact on wind farm power production and yaw actuator duty," Renewable Energy **146**, 9–15 (2020). https://doi.org/10.1016/j.renene.2019.06.122, **Google Scholar**, **Crossref**

29. J. R. Birge and F. Louveaux, *Introduction to Stochastic Programming* (Springer Science and Business Media, 2011). **Google Scholar**, **Crossref**

30. S. Brooks, A. Gelman, G. Jones, and X.-L. Meng, *Handbook of Markov Chain Monte Carlo* (CRC Press, 2011). **Google Scholar**, **Crossref**

31. M. F. Howland and J. O. Dabiri, " Influence of wake model superposition and secondary steering on model-based wake steering control with SCADA data assimilation," Energies **14**, 52 (2021). https://doi.org/10.3390/en14010052, **Google Scholar**, **Crossref**

32. Y. LeCun, Y. Bengio, and G. Hinton, " Deep learning," Nature **521**, 436 (2015). https://doi.org/10.1038/nature14539, **Google Scholar**, **Crossref**

33. J. Annoni, P. Fleming, A. Scholbrock, J. Roadman, S. Dana, C. Adcock, F. Porte-Agel, S. Raach, F. Haizmann, and D. Schlipf, " Analysis of control-oriented wake modeling tools using lidar field results," Wind Energy Sci. **3**, 819–831 (2018). https://doi.org/10.5194/wes-3-819-2018, **Google Scholar**, **Crossref**

34. C. R. Shapiro, D. F. Gayme, and C. Meneveau, " Modelling yawed wind turbine wakes: A lifting line approach," J. Fluid Mech. **841**, R1 (2018). https://doi.org/10.1017/jfm.2018.75, **Google Scholar**, **Crossref**

35. P. Lissaman, " Energy effectiveness of arbitrary arrays of wind

turbines," J. Energy **3**, 323–328 (1979). https://doi.org/10.2514/3.62441, **Google Scholar**, **Crossref**

36. H. Zong and F. Porté-Agel, " A momentum-conserving wake superposition method for wind farm power prediction," J. Fluid Mech. **889**, A8 (2020). https://doi.org/10.1017/jfm.2020.77, **Google Scholar**, **Crossref**

37. M. F. Howland, C. M. González, J. J. P. Martínez, J. B. Quesada, F. P. Larranaga, N. K. Yadav, J. S. Chawla, and J. O. Dabiri, " Influence of atmospheric conditions on the power production of utility-scale wind turbines in yaw misalignment," J. Renewable Sustainable Energy **12**, 063307 (2020). https://doi.org/10.1063/5.0023746, **Google Scholar**, **Scitation**, **ISI**

38. J. Bossuyt, M. F. Howland, C. Meneveau, and J. Meyers, " Measurement of unsteady loading and power output variability in a micro wind farm model in a wind tunnel," Exp. Fluids **58**, 1 (2017). https://doi.org/10.1007/s00348-016-2278-6, **Google Scholar**, **Crossref**

39. G. Evensen, " The ensemble Kalman filter: Theoretical formulation and practical implementation," Ocean Dyn. **53**, 343–367 (2003). https://doi.org/10.1007/s10236-003-0036-9, **Google Scholar**, **Crossref**

40. C. R. Shapiro, G. M. Starke, C. Meneveau, and D. F. Gayme, " A wake modeling paradigm for wind farm design and control," Energies **12**, 2956 (2019). https://doi.org/10.3390/en12152956, **Google Scholar**, **Crossref**

41. B. Doekemeijer, S. Boersma, L. Y. Pao, and J.-W. van Wingerden, " Ensemble Kalman filtering for wind field estimation in wind farms," in *2017 American Control Conference (ACC)* (IEEE, 2017), pp. 19–24. **Google Scholar**, **Crossref**

42. C. R. Shapiro, J. Meyers, C. Meneveau, and D. F. Gayme, " Dynamic wake modeling and state estimation for improved model-based receding horizon control of wind farms," in *2017*

model-based receding horizon control of wind farms," in 2017 *American Control Conference (ACC)* (IEEE, 2017), pp. 709–716. **Google Scholar**, **Crossref**

43. C. Schillings and A. M. Stuart, " Analysis of the ensemble Kalman filter for inverse problems," SIAM J. Numer. Anal. **55**, 1264–1290 (2017). https://doi.org/10.1137/16M105959X, **Google Scholar**, **Crossref**

44. R. J. Stevens, D. F. Gayme, and C. Meneveau, " Coupled wake boundary layer model of wind-farms," J. Renewable Sustainable Energy **7**, 023115 (2015). https://doi.org/10.1063/1.4915287, **Google Scholar**, **Scitation**, **ISI**

45. M. A. Iglesias, K. J. Law, and A. M. Stuart, " Ensemble Kalman methods for inverse problems," Inverse Probl. **29**, 045001 (2013). https://doi.org/10.1088/0266-5611/29/4/045001, **Google Scholar**, **Crossref**

46. G. M. Starke, C. Meneveau, J. R. King, and D. F. Gayme, " The area localized coupled model for analytical mean flow prediction in arbitrary wind farm geometries," arXiv:2009.13666 (2020). **Google Scholar**

47. A. S. Ghate and S. K. Lele, " Subfilter-scale enrichment of planetary boundary layer large eddy simulation using discrete Fourier–Gabor modes," J. Fluid Mech. **819**, 494–539 (2017). https://doi.org/10.1017/jfm.2017.187, **Google Scholar**, **Crossref**

48. M. F. Howland, A. S. Ghate, and S. K. Lele, " Influence of the horizontal component of earth's rotation on wind turbine wakes," J. Phys.: Conf. Ser. **1037**, 072003 (2018). https://doi.org/10.1088/1742-6596/1037/7/072003, **Google Scholar**, **Crossref**

49. M. F. Howland, A. S. Ghate, and S. K. Lele, " Influence of the geostrophic wind direction on the atmospheric boundary layer flow," J. Fluid Mech. **883**, A39 (2020). https://doi.org/10.1017/jfm.2019.889, **Google Scholar**, **Crossref**

50. M. F. Howland, A. S. Ghate, and S. K. Lele, " Coriolis effects within and trailing a large finite wind farm," in *AIAA Scitech 2020 Forum* (ARC, Reston, VA, 2020), p. 0994. **Google Scholar**, **Crossref**

51. N. S. Ghaisas, A. S. Ghate, and S. K. Lele, " Effect of tip spacing, thrust coefficient and turbine spacing in multi-rotor wind turbines and farms," Wind Energy Sci. **5**, 51–72 (2020). https://doi.org/10.5194/wes-5-51-2020, **Google Scholar**, **Crossref**

52. V. Kumar, J. Kleissl, C. Meneveau, and M. B. Parlange, " Large-eddy simulation of a diurnal cycle of the atmospheric boundary layer: Atmospheric stability and scaling issues," Water Resour. Res. **42**, W06D09, https://doi.org/10.1029/2005WR004651 (2006). **Google Scholar**, **Crossref**

53. M. Calaf, C. Meneveau, and J. Meyers, " Large eddy simulation study of fully developed wind-turbine array boundary layers," Phys. Fluids **22**, 015110 (2010). https://doi.org/10.1063/1.3291077, **Google Scholar**, **Scitation**, **ISI**

54. W. Munters, C. Meneveau, and J. Meyers, " Turbulent inflow precursor method with time-varying direction for large-eddy simulations and applications to wind farms," Boundary-Layer Meteorol. **159**, 305–328 (2016). https://doi.org/10.1007/s10546-016-0127-z, **Google Scholar**, **Crossref**

55. A. S. Ghate, N. Ghaisas, S. K. Lele, and A. Towne, " Interaction of small scale homogenenous isotropic turbulence with an actuator disk," in *2018 Wind Energy Symposium* (ARC, Reston, VA, 2018), p. 0753. **Google Scholar**, **Crossref**

56. S. Wharton and J. K. Lundquist, " Atmospheric stability affects wind turbine power collection," Environ. Res. Lett. **7**, 014005 (2012). https://doi.org/10.1088/1748-9326/7/1/014005, **Google Scholar**, **Crossref**

57. S. E. Haupt, B. Kosovic, W. Shaw, L. K. Berg, M. Churchfield, J. Cline, C. Draxl, B. Ennis, E. Koo, R. Kotamarthi *et al.*, " On bridging a modeling scale gap: Mesoscale to microscale coupling for wind energy," Bull. Am. Meteorol. Soc. **100**, 2533–2550 (2019). https://doi.org/10.1175/BAMS-D-18-0033.1, **Google Scholar**, **Crossref**

58. E. Cleary, A. Garbuno-Inigo, S. Lan, T. Schneider, and A. M. Stuart, " Calibrate, emulate, sample," J. Comput. Phys. **424**, 109716 (2021). https://doi.org/10.1016/j.jcp.2020.109716, **Google Scholar**, **Crossref**

59. A. Garbuno-Inigo, F. Hoffmann, W. Li, and A. M. Stuart, " Interacting Langevin diffusions: Gradient structure and ensemble Kalman sampler," SIAM J. Appl. Dyn. Syst. **19**, 412–441 (2020). https://doi.org/10.1137/19M1251655, **Google Scholar**, **Crossref**